Microchemical Journal 220 (2026) 116381

Contents lists available at ScienceDirect

Microchemical Journal

journal homepage: www.elsevier.com/locate/microc

Effect of environmental conditions and deposition substrate on bloodstain ageing studied by means of Raman and near infrared spectroscopies coupled with chemometrics

Sara Gariglio [a,b], Cristina Malegori [a,*], Alicja Menżyk [c,d], Grzegorz Zadora [c,d], Marco Vincenti [e], Monica Casale [a], Paolo Oliveri [a]

[a] DIFAR – Department of Pharmacy, University of Genova, Viale Cembrano 4, Genova, Italy
[b] DCCI – Department of Chemistry and Industrial Chemistry, University of Genova, Via Dodecaneso 31, Genova, Italy
[c] Institute of Chemistry, University of Silesia in Katowice, Szkolna 9, Katowice, Poland
[d] Institute of Forensic Research in Krakow, Westerplatte 9, Krakow, Poland
[e] Department of Chemistry, University of Turin, Via Pietro Giuria 7, Torino, Italy

ARTICLE INFO

Keywords:
Near infrared spectroscopy
Raman spectroscopy
Bloodstain dating
RMANOVA
Chemometrics
Forensics

ABSTRACT

The accurate estimation of bloodstain age is a critical aspect of forensic investigations, providing key insights into the chronology of events on crime scenes. Numerous techniques have been proposed for time since deposition (TSD) determination, among which spectroscopic approaches offer advantages including rapidity, reproducibility, and non-destructiveness, while maintaining analytical robustness. The present study systematically investigates the influence of environmental conditions – temperature, humidity, and illumination – and substrate type on bloodstain ageing kinetics using near-infrared (NIR) and Raman spectroscopies. Blood samples were deposited on four substrates (cotton, polyblend, glass, and metal) and aged under four controlled environmental conditions over a 12 day period, with repeated spectral measurements at fourteen time points. Partial least squares (PLS) regression was then employed to extract features representative of temporal evolution. Finally, regularised multivariate analysis of variance (RMANOVA) was used to quantify the effects of factors and their interactions. Substrate type emerged as the primary determinant of spectral variability, significantly affecting both NIR and Raman signals, while environmental conditions notably modulated ageing kinetics, with the combination of temperature and humidity exerting a greater influence on Raman measurements and illumination predominantly affecting NIR spectra. Interactions between factors were also significant, highlighting the complexity of bloodstain degradation. Comparisons with a dummy factor representing donor variability indicated that substrate and environmental conditions outweigh biological variability. These findings underscore the necessity of accounting for deposition surface and environmental conditions when developing predictive models for bloodstain dating, and suggest that robust dating may be achievable even with unknown donors, provided that experimental conditions are properly replicated.

1. Introduction

Blood has long been recognized as crucial evidence in forensic science and its importance has grown even further in recent decades due to significant advancements in DNA extraction, amplification, and sequencing [1]. Over the past 15–20 years, researchers have also directed their attention towards estimating the age of bloodstains. Determining the time since deposition (TSD) of bloodstains is, in fact, a critical aspect of forensic practice, as it provides valuable insights into the chronology of events at a crime scene. Specifically, it can help establish the time frame in which a offense was committed or determine whether a blood trace from a suspect was created before, during, or after the criminal event. Consequently, it could aid prosecutors in assessing the innocence or culpability of a suspect [2].

Several approaches have been proposed to address this issue, including quantification of RNA degradation [3,4], evaluation of aspartic acid racemization rate [5], study of the circadian hormones [6], assessment of enzyme activity [7], and measurement of fluorescence

* Corresponding author.
E-mail address: malegori@difar.unige.it (C. Malegori).

https://doi.org/10.1016/j.microc.2025.116381
Received 14 October 2025; Received in revised form 25 November 2025; Accepted 26 November 2025
Available online 28 November 2025

lifetime [8,9]. Various analytical techniques have been employed to identify an applicable method for estimating the age of bloodstains, such as high-performance liquid chromatography [10,11], electron paramagnetic resonance [12], immunoelectrophoresis [13], and atomic force microscopy [14]. However, all these techniques are often time-consuming and require sample preparation, which can lead to the destruction of the specimen. Consequently, they are suboptimal for the forensic practice, which demands timely, on-scene, and repeatable analysis. In this context, spectroscopic techniques offer significant advantages: they are fast, reproducible, non-contact, and non-destructive. Moreover, they can also be portable to some extent and research is rapidly advancing in this direction. The potential of several spectroscopies has been thoroughly reviewed by Bremmer et al. [15] and Zadora et al. [16].

Ultraviolet-visible (UV–Vis) spectroscopy was one of the first and most investigated choices for scientists studying TSD [16], as blood changes colour when exposed to air. This has been studied in both short time frames (2 days [17]) and long time frames (200 days [18]), with satisfactory results. Another well-studied technique is Raman spectroscopy, which has proven to be precise and robust over short time periods [19], although it is less efficient for TSD larger than a couple of weeks, due to increased sample fluorescence. The technique was boosted by Menżyk et al. [20], who proposed a strategy to overcome sample degradation issues due to laser exposure.

Infrared (IR) spectroscopy has also been investigated as a possible technique for bloodstain dating. The capability of mid-infrared (MIR) spectroscopy to identify functional groups and changes in protein structure makes it a promising method for studying bloodstain ageing, where the main changes are attributable to haemoglobin degradation [21]. This technique was mainly investigated in the attenuated total reflection (ATR) mode and proved useful for medium to long time periods (from two to six months from deposition) [22]. Near-infrared (NIR) spectroscopy (900–2500 nm) also turned out useful, as it can describe both protein structure and water evaporation, the two main processes characterizing blood ageing. The potential of NIR spectroscopy has been investigated in a few studies [23,24]. Notably, Gariglio et al. recently demonstrated that NIR spectroscopy can provide results comparable to those of the more established UV–Vis spectroscopy in real case scenarios [25].

Despite the undeniable advantages of spectroscopy, the technique may suffer from background interference, depending on sample presentation and wavelengths range. In forensic practice, blood is expected to be found on various surfaces, which may have a spectral signature and therefore cover up blood signals [26]. As expected, UV–Vis spectroscopy is the technique most affected by changes in background colour, while this difficulty can be overcome by using IR spectroscopy [24].

Few studies have taken into account the characteristics of the substrate and, among them, Manis et al. [23] used the NIR range coupled with hyperspectral imaging to investigate differences in blood-substrate interactions. They demonstrated that bloodstains aged on hydrophilic substrates (*e.g.*, cotton) yield better prediction results than those aged on hydrophobic substrates (*e.g.*, polyester). Moreover, Mengual-Pujante et al. [27] investigated the use of absorbent substrates (cotton, filter paper, and regular paper) by means of ATR-Fourier transform IR (ATR-FT-IR) and demonstrated that non-rigid absorbing supports are ideal for the ATR technique, since they enable the use of the sample without resuspension or risk of damage. Gautam et al. [28] applied the same approach with Raman spectroscopy to predict the TDS of bloodstains deposited on facial tissue, floor tile or linoleum, and confirmed that absorbing substrates yield better prediction results than non-absorbing ones. Mengual-Pujante et al. also showed that training regression models without taking the substrate into account, *i.e.*, including samples on cotton, paper, and filter paper in the same model, produces worse results than creating separate models for each substrate.

In light of these considerations, there is a concrete hypothesis that the background may both cause spectral interferences and modify the ageing kinetics of bloodstains, promoting or delaying chemical modifications in the sample. This last aspect is crucial, as while spectral interferences can be corrected or dealt with by chemometrics, chemical and physical modifications in blood degradation hinder the possibility of using global models to deal with different scenarios.

In the context of ageing kinetics, temperature, humidity, and light exposure are the most studied factors, and their influence on bloodstain degradation and dating have been suggested several times [16,26]. For instance, three studies [21,27,29] used ATR-FT-IR spectroscopy to develop dating models for bloodstains kept either in laboratory or outdoor conditions, but temperature and humidity were not monitored, limiting the conclusions that could be drawn about their effect. Moreover, both Mengual-Pujante et al. [27] and Lin et al. [29] stated that combining the models from outdoor and indoor samples produced worse dating performances, suggesting that the conditions may indeed modify the ageing rate. Similarly, studies using UV–Vis [30,31] and Raman spectroscopies [32,33] investigated the effect of storage temperature and/or humidity on bloodstain ageing, but these factors were analysed separately and their global effect and interaction with other factors, such as illumination or substrate, were not considered. Most of the cited studies were designed to capture as much variability of the data as possible for incorporation into a global model, while the role of individual factors in the ageing process was rarely examined. Moreover, the correlations and interactions between factors have been overlooked almost completely. This information would be extremely relevant in real case scenarios, where clear guidelines for forensic practitioners are needed in order to ensure an efficient sampling and on-scene proof collection.

An in-depth understanding of factors' effects and their interaction can be carried out by means of design of experiment (DoE) and analysis of variance (ANOVA) [34]. In particular, when dealing with multivariate datasets, such as those generated by spectroscopic techniques, methods like ANOVA simultaneous component analysis (ASCA) [35,36], multivariate ANOVA (MANOVA) [37,38] and regularised MANOVA (RMANOVA) are among the most suitable [36,38,39] for addressing the experimental factors' effect. In particular, MANOVA is a statistical method to explore factors' effect and their interrelations when samples are described with multiple variables. However, it is limited by the fact that it can only be applied when the number of samples is (much) higher than that of variables, while RMANOVA is applicable even when the number of variables is (much) larger than the number of samples [36,39]. These techniques can sometimes be combined with feature extraction, a data compression approach which consists in applying a chemometric model to summarise the information from a high number of variables in fewer new variables obtained from the combination of the original ones and containing most of their variability [40]. The model used to extract the information can be unsupervised, such as PCA [40], or supervised, such as linear discriminant analysis [41], partial least squares discriminant analysis (PLS-DA) [42], or partial least squares (PLS) regression [43].

These approaches already proved useful in several research fields, including food chemistry [44–46] and biology [47,48]. In one study, the application of ASCA on NIR spectra of honey effectively discriminated and described the effect of temperature, irradiation, adulteration and time on honey samples [49]. However, to date only one study [20] applied these techniques to a forensic framework. In particular, RMANOVA was used to determine whether an unconventional acquisition configuration in Raman spectroscopy yielded better results than the configuration commonly used for bloodstain dating. None of these techniques has been applied previously to study the effect of environmental conditions and substrate of deposition on bloodstain ageing.

Within the described context, the present study aims at analysing, quantifying and comparing the effects of climatic conditions (intended as covariation of temperature and humidity), illumination and substrate of sample deposition, in order to identify which factors or their interactions may have a significant effect on forensic bloodstains ageing

process. To reach this goal, bloodstains were deposited on four substrates (cotton, polyblend fabric, glass and metal) and aged in four different environmental conditions controlling temperature, humidity, and illumination and mimicking the real day-night alternance by means of a climatic chamber equipped with a solar lamp. The ageing of all samples was followed for two weeks – fourteen sampling times overall – by means of a portable NIR spectrophotometer and a benchtop Raman microscope. As an additional outcome, this experimental scheme allowed to study the differences in the factors' effects with respect to the chosen analytical technique. It is important to notice that, to address the significance, all the studied effects were compared to both typical statistical thresholds (*p value*) and the effect of subject, treated as a dummy factor. This data processing strategy was intended to verify if the importance of evaluating environmental conditions and substrate of deposition is greater than that of the blood donor.

2. Materials and methods

2.1. Experimental protocol and instrumentation

Blood samples were drawn by fingertip puncturing and the biological fluid was recovered with a quantitative pipette set to 20 μl and immediately deposited for analysis without the addition of any anticoagulant agent. The four backgrounds materials used for deposition were two fabric substrates, namely cotton and polyblend, one glass substrate, namely microscope glass slides (Pearl Microscope Slides, 1.0–1.2 mm thickness), and one metal substrate, namely table knife blades. Fabrics were thoroughly washed at least twice before use, to ensure comparability to used clothes. Blood was drawn in triplicates from each donor for each substrate, for a total of 2 donors × 4 substrates × 3 replicates = 24 samples.

After deposition, samples were immediately stored in a KMF 115 constant climate chamber (Binder GmbH, Tuttlingen, Germany) to age under controlled environmental conditions. Inside the storage chamber, a SUNLIGHT 430 W metal-halide lamp (SIGMA Tech, Warsaw, Poland) was located for sample irradiation. The lamp nominal power was 450 W, with a final intensity of 55 W/m^2 for UVA radiation, 10 W/m^2 for UVB, 120.000 lx for visible light and 850 W/m^2 for solar spectrum radiation.

In the present study, two climatic conditions were considered: one with lower temperature and higher humidity (cold and wet – CW) and one with higher temperature and lower humidity (hot and dry – HD). Samples illumination was performed under two different configurations, either through a glass window, mimicking indirect exposure to sunlight, as may happen within a building (inside – I), or under direct illumination, mimicking direct exposure to sunlight, as may happen in open air (outside - O). Each setup mimicked the day-night alternance in cycles of 12 h of light and 12 h of dark, switching respectively on and off the solar lamp and alternating warmer temperature and lower humidities when the lamp was on, and colder temperatures and higher humidities when the lamp was off. The conditions were combined in all possible pairs, resulting in a total of four analytical session.

The specific temperature, humidity and light configuration during day and night for each session are detailed in Table 1. All experimental conditions reported (temperature, humidity and illumination) were obtained within the KMF 115 chamber, where the samples were stored for the whole duration of the experiments, being removed only for instrumental analysis and placed immediately back afterwards.

As shown in Table 1, temperature and humidity were not treated as separate (*i.e.*, orthogonal) factors, but they covaried mimicking realistic conditions in the Mediterranean area. Therefore, the combination of these two conditions will be considered as a single factor, referred to as "T&RH" in the text. This approach was adopted to reflect real world scenarios, where temperature and humidity are always highly correlated.

The configuration of the whole experimental setting can be summarised in a full-factorial design of experiment (DoE) [34] with three qualitative factors: two in two levels (T&RH and illumination) and one in four levels (substrate). All factors and levels are reported in Table 2.

This design matrix was repeated for each of the two subjects included in the study, resulting in a total of 32 experimental conditions analysed in triplicate, making the final number of independent samples equal to 96. "Subject" may be considered as a fourth factor (SF) on two levels (A and B), though its effect is not of interest. Indeed, while it is possible that SF might have an effect on blood ageing, it is rarely controllable in real case forensic scenarios, since the blood source might be unknown or unavailable. Therefore, SF will be treated as a "dummy variable" in the present paper, *i.e.*, other factors will be considered significant only when their effect is higher than that of SF. This is done to ensure that the controllable conditions, *i.e.*, T&RH, illumination and substrate, have an effect even when the original blood donor is unknown. The studied subjects were both female, of age 31 (A) and 26 (B). The use of a higher number of subjects with more diverse characteristics is to be preferred for model development, but it was not the focus of the current paper, which is instead focused on proposing an analytical strategy and not a ready-to-use predictive model.

Samples were collected during four different analytical sessions and their ageing was followed for 12 days. They were analysed 14 times during this period, with higher frequency in the first five days after deposition and lower frequency in the following 7 days. In particular, samples were analysed after 5, 24, 29, 48, 53, 72, 77, 96, 101, 169, 193, 217, 241 and 265 h since deposition.

NIR analyses were performed using an OnSite-W MicroNIR® (VIAVI Solutions Inc., Chandler, Arizona, US) spectrophotometer, handled with the VIAVI MicroNIR™ Pro v3.2 software. The range of spectral acquisition was 908–1676 nm, with an incremental step of 6.15 nm and a total of 125 spectral points. The scan count was set to 200 and the integration time was 10 ms. Samples were analysed in triplicate each day, with slight repositioning between replicates, which were then averaged.

All measurements were operated in the transflection mode. Transflection was obtained adjusting the instrumental setup to the substrate, to preserve sample integrity and ensure repeatability of analysis while maximising signal intensity (Fig. 1). For cotton and polyblend, the

Table 2
Summary of correspondences between levels of each factor.

Factor	Factor name	Levels			
		−1	−0.33	+0.33	+1
T&RH	A	CW	/	/	HD
Illumination	B	Lamp off	/	/	Lamp on
Substrate	C	Cotton	Polyblend	Metal	Glass

Table 1
Detail of temperature, humidity and illumination conditions in the four analytical sessions.

Condition name	Day			Night		
	Temperature (°C)	Humidity (RH%)	Illumination (lamp/window)	Temperature (°C)	Humidity (RH%)	Illumination (lamp/window)
HD_O	35	60	On/no	20	75	Off/no
HD_I	35	60	On/yes	20	75	Off/yes
CW_O	20	75	On/no	10	90	Off/no
CW_I	20	75	On/yes	10	90	Off/yes

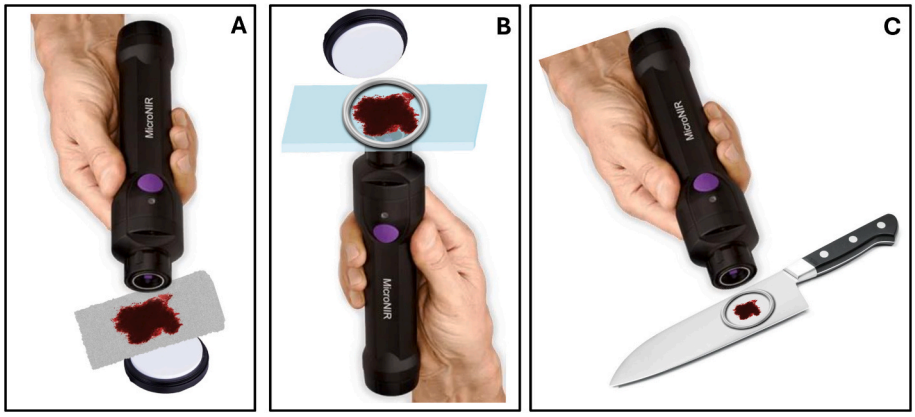

Fig. 1. Visual representation of measurement configuration for different substrates (**A**: cotton and polyblend fabric, with the Spectralon® disc beneath); **B**: glass slide with the Spectralon® disc above; **C**: metal knife). The figure shows the use of a round metal spacer to prevent the instrument from touching the specimen when it was not absorbed by the substrate and therefore subject to fracturing and damaging.

measurement was performed by placing a circular white reference material (Spectralon®, 99 % reflectance in the NIR range – radius = 2 cm) underneath the fabric and placing the MicroNIR directly on the bloodstain (Fig. 1A). For glass, the sample was placed on top of the MicroNIR and the bloodstain covered by the white reference (Fig. 1B). In both cases, the presence of the white reference ensured that the light passing through the sample would be transmitted back through to the detector. For metal, the MicroNIR was placed on top (Fig. 1C), while Spectralon® was not used, since the metal surface of the knife was sufficiently large to prevent light dispersion.

To minimise spectral variability due to unwanted fluctuations in temperature and humidity in laboratory conditions during analysis, blank substrates, *i.e.*, without bloodstains on them, were kept in the climatic chamber together with samples. Blanks were measured prior to sample analysis and every 10 min, to account for temperature/humidity changes while in laboratory conditions. Blanks (B) were analysed in the same configuration as samples and used as a "reference scan". Dark scans (D) were operated with the lamp off mode. Consequently, Transflectance (T) was calculated from sample spectra (S) as in Eq. (1):

$$T = \frac{S - D}{B - D} \quad (1)$$

This transformation also removes from the samples spectra any possible interfering trend connected to background ageing, that might otherwise have covered up for spectral trends ascribable to blood degradation.

In parallel, samples were analysed with an inVia Raman Microscope (Renishaw, New Mills, Wotton-under-Edge, Gloucestershire, UK). Spectra were recorded in the wavenumber range 150–1900 cm^{-1} with a total of 1846 wavenumbers (incremental step = 0.95 cm^{-1}). Excitation was obtained *via* a 785-nm laser line and 0.5 % of the initial laser power (68 mW) was used to irradiate the sample. The instrument was set to 3 acquisitions of 10 s each, with a total time of analysis around 7 min. Comprehensively, 96 samples × 14 sampling times = 1344 Raman spectra were measured. The microscope was used with a 50× objective (with a NA value of 0.75) and its confocal lens were manually focused each time to ensure that the detector was completely covered by the bloodstain.

2.2. Chemometric treatment

2.2.1. Data exploration

All data pre-processing, processing, and multivariate analyses were carried out using in-house scripts developed under the MATLAB® environment, version R2024b (MathWorks, Natick, MA, USA), and the PLS_Toolbox 9.5 software (Eigenvector Research Inc., Manson, WA, USA).

In order to reduce variability between spectra and to enable visualisation of spectral changes along the ageing process, spectral signatures were first analysed averaging samples without taking into account experimental conditions, obtaining a single spectrum for each time point. Then, spectra were visually inspected to identify significant bands and regions connected to ageing. Both the NIR and Raman datasets underwent the same chemometric processing, while different pre-processing techniques and different combination of them were tested for the two techniques in order to enhance differences among spectra and to minimise unwanted signal variations. In particular, the standard normal variate (SNV) transform [50], Savitzky-Golay first and second derivative (2nd order polynomial, 9 points window) [51], normalisation to unit length and to unit area were tested for NIR spectroscopy, while the same transforms coupled with baseline correction *via* asymmetric least squares (AsLS) smoothing or automatically weighted least squares (AWLS) [52] were used for Raman.

Then, principal component analysis (PCA) [53,54] was applied on both datasets. Score plots were inspected to investigate grouping and clustering within the data and to individuate factors responsible for the main directions of variability, while loading plots were analysed to identify spectral variables related to each factor.

2.2.2. Feature extraction

To study the effect of factors on bloodstain ageing, each sample, *i.e.*, a bloodstain in one level of substrate, T&RH, light and SF, needed to be described by a single signal representing its whole evolution along time, from sampling point 1 to 14. The signals obtained for all levels of all factors could then be compared with chemometric strategies, ruling out the effect of each factor on blood degradation.

In the present study, PLS regression [55,56] was used as a feature extraction technique, with the aim of focusing on spectral variations related to time elapsing. To do so, a regression model was built for each condition, for a total of 16 models. The calculation of individual PLS models for each condition allowed to extract time trend information without smoothing out the effect of the other factors. Each model was cross-validated with a Venetian-blind scheme with 5 blocks. The choice of pre-processing and number of significant latent variables (LVs) was done for each model by observing the trend of root mean square error in cross-validation (RMSECV) and comparing it to that of root mean square error in calibration (RMSEC). Since different models may be built with a different number of significant latent variables, the final number of latent variables (n) was homogeneously set to the minimum number of latent variables obtained from the 16 models, in order to grant the most parsimonious models and minimise the risk of overfitting. Finally, the scores on the n lowest-order LVs for each of the 14 sampling times for

each subject were concatenated, thus obtaining a new signal made of $n \times 14$ variables. For a matter of clarity, the feature extraction process is visually represented in Fig. 2.

To ensure the robustness of the approach, *i.e.*, to verify that all the significant information was indeed contained in the n lowest-order LVs, the approach was repeated three times, increasing n by 1 each time.

The final data matrix for each instrument contained 32 rows (16 conditions × 2 subjects) and $n \times$ LVs columns. This matrix was used for all further data analysis.

2.2.3. Application of RMANOVA

The data matrix was then subjected to regularised multivariate analysis of variance (RMANOVA).

In the present study, RMANOVA was applied to the data matrix to determine the statistical significance of single factors and their binary interactions. Significance was tested using the Wilks lambda distribution [57,58], whose theoretical shape was calculated through a permutation test with 10,000 permutations. A factor was considered significant if $p < 0.01$, while *p values* between 0.01 and 0.05 were considered as slightly significant. Final *p values* were calculated using Bonferroni multiple testing correction [59,60]. Moreover, a factor was considered statistically significant only if its *p value* was both significant and lower than that of SF, both alone and in combination with the other factors. Therefore, factors were significant if $p < 0.01$ and $p < p_{dummy}$. In addition, the factor percentage effect was calculated based on the amount of variance explained by the factor itself.

3. Results and discussion

3.1. Data exploration

3.1.1. Profiles observation

Visual inspection of bloodstains through the microscope associated to the Raman apparatus did not show inhomogeneity of the samples. This outcome was confirmed by the Raman spectra obtained from preliminary results, which demonstrated consistency between three repeated measurements taken in different regions within the same sample (data not shown). Conversely, the NIR spectrometer naturally accounts for this possibility, considering an average signal of the whole bloodstain, thanks to the big diameter of the probe (~1 cm).

After homogeneity evaluation, the evolution of spectra over time was analysed for both NIR and Raman techniques to visually confirm their ability to describe the ageing process. To this aim, Fig. 3 shows the time evolution of spectra averaged for session, T&RH, substrate and SF.

Both NIR and Raman spectra already showed clear time dependence when raw signals were considered, as the progressive change in colour from blue (fresh samples) to yellow (aged samples), evidenced in each subplot of the figure, demonstrates. In particular, NIR presented a total intensity effect (Fig. 3A), with aged samples presenting lower transflectance values compared to fresh ones. This effect is most probably a result of the combined effect of water evaporation due to sample drying over time, colour darkening and scattering changes owing to the cracking of bloodstains. The application of SNV (Fig. 3B) evidenced the

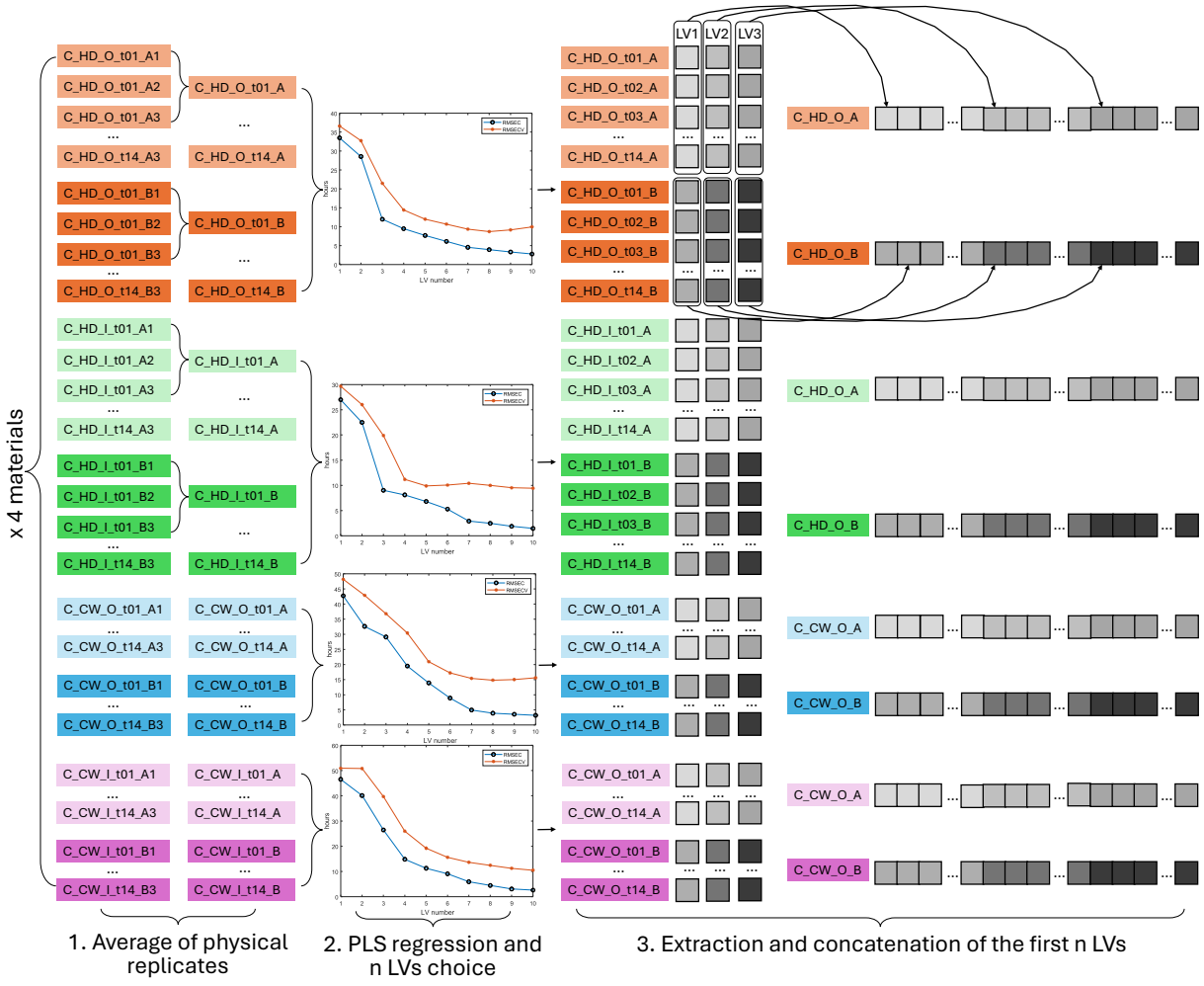

Fig. 2. Schematic representation of the features extraction process, exemplified on substrate = cotton. The same scheme was repeated for all four materials and for both instruments.

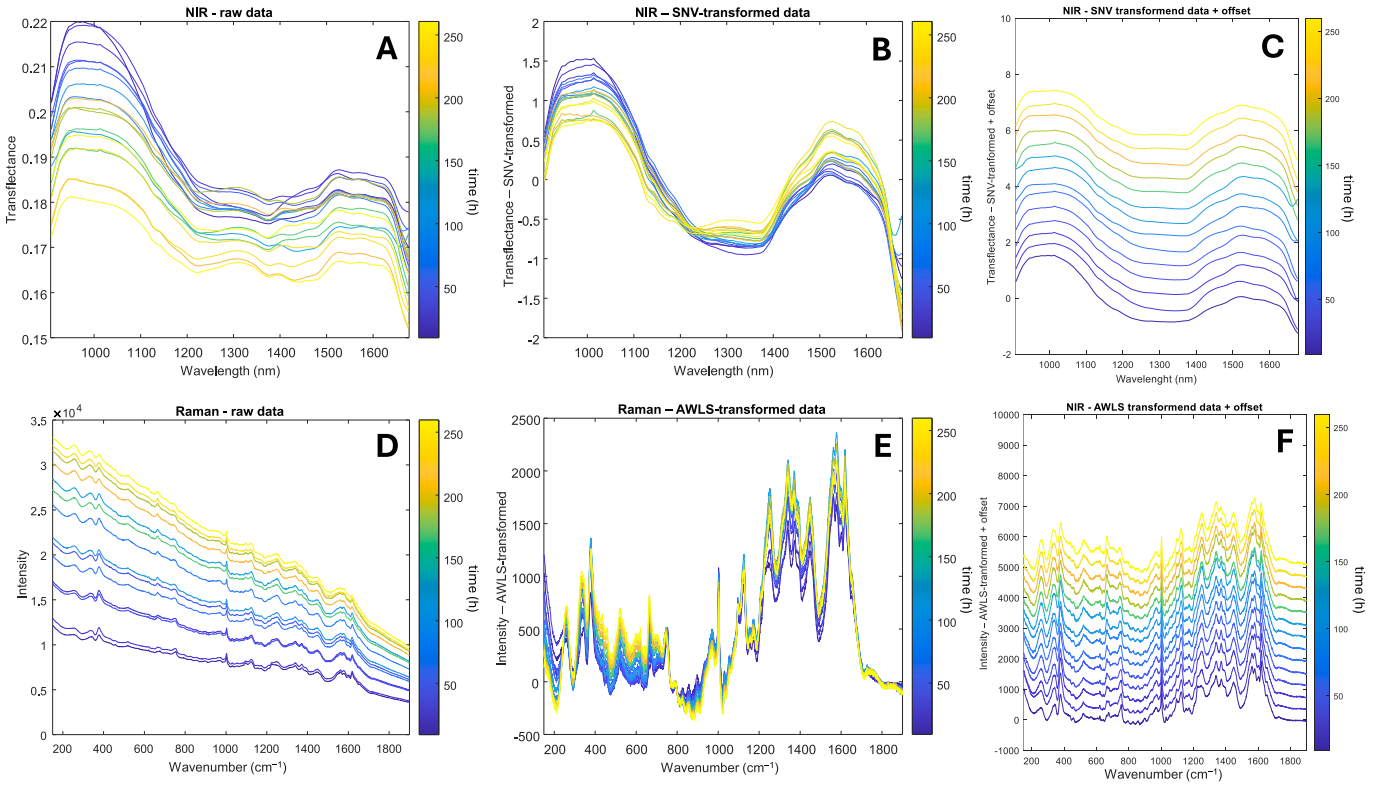

Fig. 3. Spectral profiles of samples averaged over time. **A**: raw NIR spectra; **B**: SNV transformed NIR spectra; **C**: SNV transformed NIR spectra with offset; **D**: raw Raman spectra; E: AWLS transformed Raman spectra; F: AWLS transformed Raman spectra with offset. Spectra are colour coded according to sampling time in hours.

effect of time even more, underlining the continuous change in spectral feature in relation to sampling time, and showing the presence of a strong absorbing region between 1200 and 1400 nm, relative to the second overtone of OH stretching. Moreover, the use of background samples aged in parallel with the blood samples and used as reference in the reflectance calculation (see Eq. (1)) ensured that blood ageing was the only responsible for the time trends revised in the spectra, effectively eliminating the interference connected to possible background ageing during the analysis duration. To clearly visualise the changes in spectral features, in Fig. 3C SNV transformed spectra were also represented with a constant offset.

Moving to Raman spectroscopy, Fig. 3D shows a clear total intensity effect coupled with a multiplicative effect related to the time trend, with aged samples presenting higher count values due to increased fluorescence in aged blood samples, as already reported in the literature [20,61–63]. One possible explanation for this phenomenon is the accumulation of haemoglobin (Hb) degradation products that have stronger natural fluorescence than oxyhaemoglobin (oxyHb), which is the main form found in fresh blood. According to previous studies [64–66], one of these fluorescent Hb byproducts is hemichrome, which has been identified as a result of natural blood degradation [62] and shows strong fluorescence [67]. Moreover, it is possible that further degradation continues over time, leading to the formation of other heavily degraded Hb forms showing fluorescent properties, possibly caused by the cleavage of its subunits and release of iron ions [64–66].

Compared to what commented for NIR spectroscopy, raw Raman spectra presented low to no background influence, with the exception of cotton which, being an absorbent substrate, presented a moderate background signal mixed with the blood signal. For this reason, it was easier in this case to proceed with spectral interpretation and band attribution, after an appropriate correction of the baseline effect due to fluorescence.

In particular, after application of baseline correction by means of AWLS, age-dependent spectral alterations become more evident, as represented in Fig. 3E. These spectral changes, particularly evident within the 300–1700 cm^{-1} region, provide molecular insight into the degradation pathways of haemoglobin and represent valuable markers for estimating the bloodstains age in forensic applications [20,62,68]. Notably, the band around 377–380 cm^{-1}, attributed to vibrational modes characteristic of methaemoglobin (metHb), shows a progressive increase in intensity over time, reflecting the gradual auto-oxidation of oxyHb to metHb during blood degradation. This band serves as a sensitive marker for the presence of high-spin ferric heme species formed during the ageing process [62,69]. In the 900–1000 cm^{-1} region, some changes may occur in the relative intensities of the bands at approximately 976 cm^{-1} and 1003 cm^{-1}. The band near 976 cm^{-1}, associated with heme aggregation and degradation products, increases in intensity relative to the phenylalanine ring-breathing mode at 1003 cm^{-1}, which remains relatively stable. The ratio of the intensities of these two bands (976/1003 cm^{-1}) therefore serves as an additional metric to discriminate between differently aged bloodstains, indicating progressive heme aggregation and structural changes within haemoglobin derivatives. Notably, bands associated with non-heme components of Hb, such as the amide I band at *ca.* 1655 cm^{-1}, exhibit minimal variability over time. Their relative stability suggests that protein backbone remain largely unaffected during the early stages of *ex vivo* degradation, while the observed spectral changes primarily originate from the heme prosthetic group and its immediate environment. To clearly visualise the changes in spectral features, in Fig. 3F AWLS transformed spectra were also represented with a constant offset.

These findings highlight the suitability of Raman spectroscopy to support the time evolution observed by NIR spectroscopy, with both techniques offering a valuable framework for tracking the influence of external factors on the ageing process of bloodstains, to be supported by multivariate analysis techniques.

3.1.2. PCA

The data exploration continued with the application of PCA, which

was used to identify groupings within the data and to make an initial evaluation of the main sources of variability for the two techniques. Fig. 4 shows the results, displaying the score plots for both NIR (Fig. 4A-C) and Raman (Fig. 4E-G) spectroscopies, coloured according to the three analysed factors. The associated loading plots are shown in Fig. 4D and H.

The score plots obtained for NIR spectroscopy revealed that the main source of variability was the difference between substrates (Fig. 4A). In particular, PC1 differentiated between fabric substrates (cotton and polyblend) and non-absorbing substrates (glass and metal), while PC2 differentiated cotton from all the other substrates. PC1 loadings explain a total intensity effect, indicating different global reflectance of the substrates and summarising the physical effect of light on the material. This justifies the distinction between fabrics and non-absorbing substrates, the former being less reflective than the latter. PC2 loadings mostly relate to bands and explain the chemical differences between substrates. A shift was visible to some extent also for T&RH and illumination along both PC1 and PC2 (Fig. 4B & 4C), suggesting that the effects of these two factors are also connected to chemical and physical effects.

In Raman spectroscopy, the main source of variability is more subtle. Fig. 4E shows the effect of the substrate, in which only cotton forms a clear cluster at negative values of PC1 and PC2, while the other three materials overlap, covering the remaining PC space. Differences can also be observed when the T&RH factor is considered (Fig. 4F), with samples from the HD level (red in the figure) showing higher values of PC1 and lower values of PC2 than the CW samples (green in the figure). Conversely, grouping is not observed for the illumination factor. In the loading plot (Fig. 4G), PC1 explains a combined total intensity and multiplicative effect due to fluorescence, as discussed in Section 3.1.1, while PC2 reflects both a baseline shift and a multiplicative effect.

The choice of presenting PCA on raw data was made to avoid possible interferences or artefacts due to the algebraic pre-processing transformations [70]. However, PCA results for both NIR and Raman spectroscopies were also confirmed on pre-processed data, as shown in the Supplementary Material (**Fig. S1**). As mentioned above, it was possible to observe that the main source of variability in Raman spectroscopy on raw data was not due to one of the analysed factors, but rather to the time trend, as can be seen in **Fig. S2B** of the Supplementary Material. This could also be deduced from the fact that PC1 on raw data explains the information related to fluorescence, which is the main source of variability connected to time trend, as already discussed in Section 3.1.1. On the contrary, ageing information was not evident in the NIR raw data, but could be enhanced through pre-processing, as shown in **Fig. S2A** and **S2C** (Supplementary Material). Pre-processing enhanced the variability due to the substrate in Raman spectroscopy, masking that due to time. The loadings shown in **Fig. S1G** (Supplementary Material) also allowed the peaks responsible for the difference between cotton and the other substrates in Raman spectroscopy to be identified, thanks to the information on PC2. However, PCA was insufficient to deconvolute the information related to factors and their significance, suggesting the use of more targeted variance deconvolution techniques.

3.2. Factors analysis

3.2.1. Extraction of principal properties

As described in Section 2.2.2, feature extraction was performed using PLS regression. A regression model to estimate time was trained for each of the sixteen conditions for both instruments, resulting in a total of 32 regression models. The figures of merit of the calculated models are reported in **Tables S1** and **S2** in the Supplementary Material for NIR and Raman spectroscopies, respectively, and show that the minimum number of latent variables across all models was 3. For NIR spectroscopy, the best pre-processing was first derivative followed by SNV transform for cotton, metal and polyblend substrates and just SNV transform for the glass substrate. For Raman, the best approach was to use raw data for all conditions. Although the aim of the regression step was not to produce a predictive dating model for different conditions, but rather to extract features to use in the next step, the models' performance was adequate to proceed.

The comparison of model performances provides interesting information about the differences between the information content yielded by the two analytical techniques. NIR spectroscopy performed particularly well on absorbing substrates, in particular on cotton, followed by polyblend, which has an intermediate absorbing capacity. The worst-performing models, obtained on metal, is justified by the high reflection and scattering of metal surfaces, which perturbs the NIR spectra and hinders their regression capabilities. Conversely, Raman spectroscopy performed well on non-absorbing substrates, as evidenced by the comparable errors in cross-validation for glass, metal and polyblend, while cotton yielded the worst performance, as evidenced by the highest RMSECV values, particularly under HD conditions.

3.2.2. RMANOVA

The application of RMANOVA enabled the deconvolution of the significance of factors and their interactions, as demonstrated in Table 3. In particular, the substrate resulted to be the most significant, for both NIR and Raman spectroscopies. This factor accounts for the largest part of the variance and confirms the trends observed in PCA (Section 3.1.2).

To better interpret results discussed in Table 3, **Fig. S3** (Supplementary Material) supports the conclusions by showing the dispersion of data points coloured according to factors levels in the canonical variate (CV) space. The figure also presents the average spectra for each level. From this figure, it is possible to note that all levels are grouped within the space, and no overlap is detected. This contrasts with some of the observations drawn from PCA. For instance, when considering **Fig. S3C**, referred to the effect of substrate analysed with Raman spectroscopy, cotton retains the highest difference, as can be noticed by its position on the CV1, but the other three levels also present a grouping. Conversely, in PCA the only level presenting a grouping was cotton. However, when examining **Fig. S3B**, representing the average spectra for the four levels of substrate, cotton is the only one exhibiting a different spectral signature. This suggests that the effect underlined by in RMANOVA is likely attributable to a distinct temporal evolution, which remained undetectable when analysing the spectral signatures as such. This result suggests that the interaction between substrate and blood may be able to modify the ageing kinetics of blood itself, having a stronger effect on the evolution of the signal over time than on specific bands.

The effect of temperature and humidity (T&RH) proved significant with both techniques, but it was slightly more pronounced for Raman spectroscopy, in agreement with PCA results. In NIR spectroscopy, the effect of T&RH was not readily discernible neither in PCA nor by visual examination of the average spectrum. The findings of the present study confirm that, indeed, temperature and humidity conditions have a significant impact on the rate of blood ageing kinetics.

The direct exposure of bloodstains to light proved to have a significant effect only on NIR spectra. In particular, its influence was the second most important, after the substrate's, whereas Raman spectra were apparently unaffected by different illumination conditions. The different outcome observed with the two spectroscopic techniques is justified by assuming that the main effect of direct illumination is to promote the water evaporation rate, when temperature and humidity are kept constant. The high sensitivity of NIR spectroscopy towards the water content is therefore influenced by an accelerated sample drying. In contrast, Raman spectra are unaffected by the illumination conditions, since they do not present any characteristic water band. Likewise, binary interaction factors involving the illumination conditions proved significant only in NIR spectroscopy, whereas in Raman spectroscopy only the binary factors unrelated to illumination proved significant.

From a statistical perspective, it is evident that, virtually, all the experimental conditions tested (substrate, T&RH, illumination) produced a significant effect on the kinetics of bloodstain ageing. Moreover,

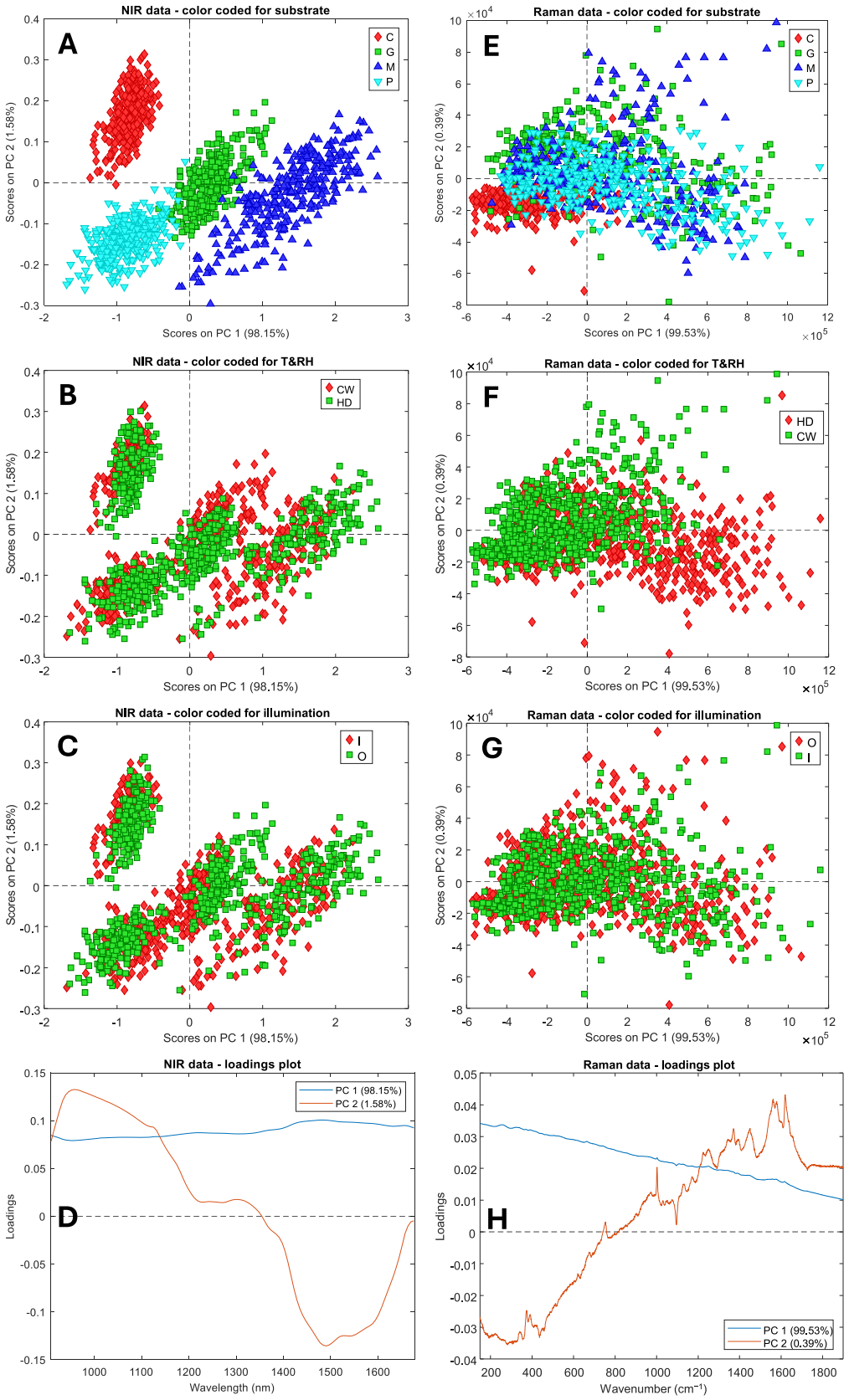

Fig. 4. Score and loading plots obtained from PCA on raw data both for NIR and Raman spectroscopy, colour coded for the different factors and levels under analysis. **A**: NIR score plot colour coded according to substrate (C = cotton, G = glass, M = metal, P = polyblend fabric); **B**: NIR score plot colour coded according to T&RH; **C**: NIR score plot colour coded according to illumination; **D**: NIR loading plot; **E**: Raman score plot colour coded according to substrate (C = cotton, G = glass, M = metal, P = polyblend fabric); **F**: Raman score plot colour coded according to T&RH; **G**: Raman score plot colour coded according to illumination; H: Raman loading plot.

Table 3
Summary of RMANOVA results for NIR and Raman spectroscopies. Cells with a grey background refer to results for the dummy variable. ** = $p < 0.01$; * = $p < 0.01$ and $Effect_{factor} > Effect_{dummy}$.

Factor	NIR		Raman	
	Effect (%)	*p value*	Effect (%)	*p value*
Dummy	2.4	0.026*	3.4	0.046*
Dummy × substrate	4.5	0.51	4.5	0.87
Dummy × T&RH	0.6	0.96	3.7	0.03*
Dummy × illumination	0.5	0.99	3.4	0.046*
Substrate	33.2	0.00001**	46.5	0.00001**
T&RH	5.2	0.0002**	12.5	0.00001**
Illumination	7.0	0.00001**	2.3	0.29
Substrate × T&RH	22.6	0.00001**	13.9	0.0009**
Substrate × illumination	18.4	0.00001**	7.9	0.088
T&RH × illumination	5.6	0.0002**	2.1	0.4

these effects exhibited a magnitude that widely exceeded that of the dummy variable, whose significance was found in the range $0.02 < p < 0.05$. This comparison underscores the paramount importance of the environmental conditions, whose effects – broadly surpassing the biological variability of bloodstains collected from different individuals – should be strictly controlled in whatever statistical model built to evaluate the bloodstain ageing.

4. Conclusions

The present study applied a systematic DoE approach and variance deconvolution to facilitate a comprehensive understanding of the significance and interaction of the factors influencing bloodstain ageing kinetics, including environmental conditions and deposition substrate.

The central role of the substrate on which the bloodstain is deposited is particularly salient in the forensics context, emphasising the constraint of producing dating models that utilise the same substrate background on which evidence is deposited in order to attain reliable predictions. This warning has practical implications for forensic practitioners, who are advised to consider the bloodstains together with their background, without removing or separating them.

Moreover, the significance of temperature, humidity, and illumination conditions was clearly demonstrated, confirming previous more qualitative observations from different studies [27–29]. The potential bias arising from the environmental conditions indicates again the need for forensic researchers to evolve towards the development of tailored models elaborated under conditions that accurately replicate the environment in which the real bloodstain samples have been exposed from the time of their deposition to the beginning of the spectroscopic measurements.

This study also evidenced that the choice of the spectroscopic technique to be used is not univocal and may depend on the sample conditions. For instance, NIR spectroscopy appeared to be suitable for the analysis of blood deposited on absorbing substrates, but may produce equivocal results when applied to non-absorbing ones. Likewise, NIR appeared to be more susceptible than Raman spectroscopy to the effects of illumination, which means that NIR spectroscopy should be applied under an accurate control of lighting on the samples during experimentation. These preliminary deductions should be further confirmed in dedicated studies.

CRediT authorship contribution statement

Sara Gariglio: Writing – original draft, Visualization, Software, Methodology, Investigation, Formal analysis, Data curation. **Cristina Malegori:** Writing – review & editing, Project administration, Methodology, Data curation, Conceptualization. **Alicja Menżyk:** Writing – review & editing, Investigation, Formal analysis, Data curation, Conceptualization. **Grzegorz Zadora:** Writing – review & editing, Supervision, Resources, Conceptualization. **Marco Vincenti:** Writing – review & editing, Conceptualization. **Monica Casale:** Writing – review & editing, Supervision. **Paolo Oliveri:** Writing – review & editing, Visualization, Supervision, Resources, Funding acquisition, Conceptualization.

Declaration of competing interest

The authors declare that they have no known competing financial interests or personal relationships that could have appeared to influence the work reported in this paper.

Acknowledgements

Financial support provided by the Italian Ministry of Universities and Research – MUR is gratefully acknowledged. Research Project PRIN 2022 n. 20223WBTH8, CUP: D53D23008950006; Research Project PRIN 2022 PNRR n. P20227N5YZ, CUP: J53D23014500001, D53D23016770001.

The work of Alicja Menżyk and Grzegorz Zadora was also funded by the Institute of Forensic Research in Krakow, project no. *V/K/* 2021–2025.

The role of Kevin Pistoia as proofreader is kindly acknowledged.

Appendix A. Supplementary data

Supplementary data to this article can be found online at https://doi.org/10.1016/j.microc.2025.116381.

Data availability

Data will be made available on request.

References

[1] C.D. Adam, Fundamental studies of bloodstain formation and characteristics, Forensic Sci. Int. 219 (2012) 76–87, https://doi.org/10.1016/J.FORSCIINT.2011.12.002.
[2] C. Weyermann, O. Ribaux, Situating forensic traces in time, Sci. Justice 52 (2012) 68–75, https://doi.org/10.1016/J.SCIJUS.2011.09.003.
[3] S. Anderson, B. Howard, G.R. Hobbs, C.P. Bishop, A method for determining the age of a bloodstain, Forensic Sci. Int. 148 (2005) 37–45, https://doi.org/10.1016/J.FORSCIINT.2004.04.071.
[4] M. Bauer, S. Polzin, D. Patzelt, Quantification of RNA degradation by semi-quantitative duplex and competitive RT-PCR: a possible indicator of the age of bloodstains? Forensic Sci. Int. 138 (2003) 94–103, https://doi.org/10.1016/J.FORSCIINT.2003.09.008.
[5] S. Arany, S. Ohtani, Age estimation of bloodstains: a preliminary report based on aspartic acid racemization rate, Forensic Sci. Int. 212 (2011) e36–e39, https://doi.org/10.1016/J.FORSCIINT.2011.05.015.
[6] K. Ackermann, K.N. Ballantyne, M. Kayser, Estimating trace deposition time with circadian biomarkers: a prospective and versatile tool for crime scene reconstruction, Int. J. Leg. Med. 124 (2010) 387–395, https://doi.org/10.1007/S00414-010-0457-1/FIGURES/5.
[7] A. Tsutsumi, Y. Yamamoto, H. Ishizu, Determination of the age of bloodstains by enzyme activities in blood cells, Japanese J. Leg. Med. 37 (1983) 770–776. https://okayama.elsevierpure.com/en/publications/determination-of-the-age-of-bloodstains-by-enzyme-activities-in-b (accessed June 4, 2025).
[8] K. Guo, S. Achilefu, M.Y. Berezin, Dating bloodstains with fluorescence lifetime measurements, Chemistry 18 (2012) 1303, https://doi.org/10.1002/CHEM.201102935.
[9] S. Mc Shine, K. Suhling, A. Beavil, B. Daniel, N. Frascione, The applicability of fluorescence lifetime to determine the time since the deposition of biological stains, Anal. Methods 9 (2017) 2007–2013, https://doi.org/10.1039/C6AY03099H.
[10] H. Inoue, F. Takabe, M. Iwasa, Y. Maeno, Y. Seko, A new marker for estimation of bloodstain age by high performance liquid chromatography, Forensic Sci. Int. 57 (1992) 17–27, https://doi.org/10.1016/0379-0738(92)90041-T.
[11] J. Andrasko, The estimation of age of bloodstains by HPLC analysis, J. Forensic Sci. 42 (1997) 601–607, https://doi.org/10.1520/JFS14171J.
[12] Y. Fujita, K. Tsuchiya, S. Abe, Y. Takiguchi, S.I. Kubo, H. Sakurai, Estimation of the age of human bloodstains by electron paramagnetic resonance spectroscopy: long-term controlled experiment on the effects of environmental factors, Forensic Sci. Int. 152 (2005) 39–43, https://doi.org/10.1016/J.FORSCIINT.2005.02.029.

[13] K. Rajamannar, Determination of the age of bloodstains using Immunoelectrophoresis, J. Forensic Sci. 22 (1977) 159–164, https://doi.org/10.1520/JFS10381J.

[14] S. Strasser, A. Zink, G. Kada, P. Hinterdorfer, O. Peschel, W.M. Heckl, A.G. Nerlich, S. Thalhammer, Age determination of blood spots in forensic medicine by force spectroscopy, Forensic Sci. Int. 170 (2007) 8–14, https://doi.org/10.1016/J.FORSCIINT.2006.08.023.

[15] R.H. Bremmer, K.G. De Bruin, M.J.C. Van Gemert, T.G. Van Leeuwen, M.C. G. Aalders, Forensic quest for age determination of bloodstains, Forensic Sci. Int. 216 (2012) 1–11, https://doi.org/10.1016/J.FORSCIINT.2011.07.027.

[16] G. Zadora, A. Menżyk, In the pursuit of the holy grail of forensic science – spectroscopic studies on the estimation of time since deposition of bloodstains, TrAC Trends Anal. Chem. 105 (2018) 137–165, https://doi.org/10.1016/J.TRAC.2018.04.009.

[17] H. Sun, Y. Dong, P. Zhang, Y. Meng, W. Wen, N. Li, Z. Guo, Accurate age estimation of bloodstains based on visible reflectance spectroscopy and Chemometrics methods, IEEE Photonics J. 9 (2017), https://doi.org/10.1109/JPHOT.2017.2651580.

[18] G. Edelman, T.G. van Leeuwen, M.C.G. Aalders, Hyperspectral imaging for the age estimation of blood stains at the crime scene, Forensic Sci. Int. 223 (2012) 72–77, https://doi.org/10.1016/J.FORSCIINT.2012.08.003.

[19] K.C. Doty, G. McLaughlin, I.K. Lednev, A. Raman, "Spectroscopic clock" for bloodstain age determination: the first week after deposition, Anal. Bioanal. Chem. 408 (2016) 3993–4001, https://doi.org/10.1007/S00216-016-9486-Z/FIGURES/5.

[20] A. Menżyk, A. Damin, A. Martyna, E. Alladio, M. Vincenti, G. Martra, G. Zadora, Toward a novel framework for bloodstains dating by Raman spectroscopy: how to avoid sample photodamage and subsampling errors, Talanta 209 (2020) 120565, https://doi.org/10.1016/J.TALANTA.2019.120565.

[21] N.F.N. Hassan, D.D. Sandran, M. Mohamad, Y. Zakaria, N.Z.M. Muslim, Estimation of the age of bloodstains on soil matrices by ATR-FTIR spectroscopy and chemometrics, international Journal of innovative technology and exploring, Engineering 9 (2019) 4750–4755, https://doi.org/10.35940/IJITEE.A4454.119119.

[22] R. Kumar, K. Sharma, V. Sharma, Bloodstain age estimation through infrared spectroscopy and Chemometric models, Sci. Justice 60 (2020) 538–546, https://doi.org/10.1016/J.SCIJUS.2020.07.004.

[23] C. Manis, C. Malegori, E. Alladio, M. Vincenti, P. Garofano, F. Barni, A. Berti, P. Oliveri, Non-destructive age estimation of biological fluid stains: an integrated analytical strategy based on near-infrared hyperspectral imaging and multivariate regression, Talanta 245 (2022) 123472, https://doi.org/10.1016/J.TALANTA.2022.123472.

[24] G. Edelman, V. Manti, S.M. Van Ruth, T. Van Leeuwen, M. Aalders, Identification and age estimation of blood stains on colored backgrounds by near infrared spectroscopy, Forensic Sci. Int. 220 (2012) 239–244, https://doi.org/10.1016/J.FORSCIINT.2012.03.009.

[25] S. Gariglio, C. Malegori, A. Menżyk, G. Zadora, M. Vincenti, M. Casale, P. Oliveri, Determination of time since deposition of bloodstains through NIR and UV–vis spectroscopy – a critical comparison, Talanta 278 (2024), https://doi.org/10.1016/J.TALANTA.2024.126444.

[26] G.J. Edelman, M. Roos, A. Bolck, M.C. Aalders, Practical Implementation of Blood Stain Age Estimation Using Spectroscopy, IEEE J. Selected Top. Quantum Electron. 22 (n.d.). doi:https://doi.org/10.1109/JSTQE.2016.2536655.

[27] M. Mengual-Pujante, A.J. Perán, A. Ortiz, M.D. Pérez-Cárceles, Estimation of human bloodstains time since deposition using ATR-FTIR spectroscopy and chemometrics in simulated crime conditions, Chemom. Intel. Lab. Syst. 251 (2024) 105172, https://doi.org/10.1016/J.CHEMOLAB.2024.105172.

[28] R. Gautam, D. Peoples, K. Jansen, M. O'Connor, G. Thomas, S. Vanga, I.J. Pence, A. Mahadevan-Jansen, Feature selection and rapid characterization of bloodstains on different substrates, Appl. Spectrosc. 74 (2020) 1238–1251, https://doi.org/10.1177/0003702820937776.

[29] H. Lin, Y. Zhang, Q. Wang, B. Li, P. Huang, Z. Wang, Estimation of the age of human bloodstains under the simulated indoor and outdoor crime scene conditions by ATR-FTIR spectroscopy, Sci. Rep. 7 (2017) 1–9, doi:10.1038/S41598-017-13725–1;TECHMETA=140,141;SUBJMETA=45,631,92;KWRD=BIOCHEMISTRY,CHEMICAL+BIOLOGY.

[30] E.K. Hanson, J. Ballantyne, A blue spectral shift of the hemoglobin Soret band correlates with the age (time since deposition) of dried bloodstains, PloS One 5 (2010) e12830, https://doi.org/10.1371/JOURNAL.PONE.0012830.

[31] K. Rampete, C.I. Elliott, T. Stotesbury, Monitoring the solid-state VIS profiles of degrading bloodstains, Forensic Chem. 35 (2023) 100507, https://doi.org/10.1016/J.FORC.2023.100507.

[32] R. Zhang, P. Wang, J. Chen, Y. Tian, J. Gao, Age estimation of bloodstains based on Raman spectroscopy and chemometrics, Spectrochim. Acta A Mol. Biomol. Spectrosc. 290 (2023), https://doi.org/10.1016/j.saa.2022.122284.

[33] H. Sun, Y. Meng, P. Zhang, Y. Li, N. Li, C. Li, Z. Guo, Non-invasive prediction of bloodstain age using the principal component and a back propagation artificial neural network, Laser Phys. Lett. 14 (2017), https://doi.org/10.1088/1612-202X/AA7C48.

[34] R. Leardi, Experimental design in chemistry: a tutorial, Anal. Chim. Acta 652 (2009) 161–172, https://doi.org/10.1016/J.ACA.2009.06.015.

[35] C. Bertinetto, J. Engel, J. Jansen, ANOVA simultaneous component analysis: a tutorial review, Anal Chim Acta X 6 (2020) 100061, https://doi.org/10.1016/J.ACAX.2020.100061.

[36] J. Jansen, J. Engel, ASCA: the implementation of Design of Experiments into Multivariate Modelling in Chemometrics, Compr. Anal. Chem. 82 (2018) 301–335, https://doi.org/10.1016/bs.coac.2018.08.007.

[37] L. Sthle, S. Wold, Multivariate analysis of variance (MANOVA), Chemom. Intel. Lab. Syst. 9 (1990) 127–141, https://doi.org/10.1016/0169-7439(90)80094-M.

[38] C. Chatfield, A.J. Collins, The multivariate analysis of variance, in: C. Chatfield, M. Tanner, J. Zidek (Eds.), Introduction to Multivariate Analysis, Chapman & Hall/CRC, 1981, pp. 140–160, https://doi.org/10.2307/3616628.

[39] J. Engel, K.J. Houthuijs, V. Vasiliou, G. Charkoftaki, Regularized multivariate analysis of variance, Comprehensive Chemometrics: Chemical and Biochemical Data Analysis, Second Edition: Four Volume Set 1 (2020) 479–494. doi:https://doi.org/10.1016/B978-0-12-409547-2.14577-9.

[40] H. Parastar, P. Weller, Feature selection and extraction strategies for non-targeted analysis using GC-MS and GC-IMS: a tutorial, Anal. Chim. Acta 1343 (2025) 343635, https://doi.org/10.1016/J.ACA.2025.343635.

[41] B. Ghojogh, M.N. Samad, S.A. Mashhadi, T. Kapoor, W. Ali, F. Karray, M. Crowley, Feature selection and feature extraction in pattern analysis: A Literature Review, (2019). https://arxiv.org/pdf/1905.02845 (accessed May 28, 2025).

[42] L.C. Lee, C.Y. Liong, A.A. Jemain, Partial least squares-discriminant analysis (PLS-DA) for classification of high-dimensional (HD) data: a review of contemporary practice strategies and knowledge gaps, Analyst 143 (2018) 3526–3539, https://doi.org/10.1039/C8AN00599K.

[43] X.S. Gan, J.S. Duanmu, J.F. Wang, W. Cong, Anomaly intrusion detection based on PLS feature extraction and core vector machine, Knowl Based Syst 40 (2013) 1–6, https://doi.org/10.1016/J.KNOSYS.2012.09.004.

[44] P. Firmani, R. Vitale, C. Ruckebusch, F. Marini, ANOVA-simultaneous component analysis modelling of low-level-fused spectroscopic data: a food chemistry case-study, Anal. Chim. Acta 1125 (2020) 308–314, https://doi.org/10.1016/J.ACA.2020.05.059.

[45] M. Ryckewaert, N. Gorretta, F. Henriot, F. Marini, J.M. Roger, Reduction of repeatability error for analysis of variance-simultaneous component analysis (REP-ASCA): application to NIR spectroscopy on coffee sample, Anal. Chim. Acta 1101 (2020) 23–31, https://doi.org/10.1016/J.ACA.2019.12.024.

[46] C. Buvé, W. Saeys, M.A. Rasmussen, B. Neckebroeck, M. Hendrickx, T. Grauwet, A. Van Loey, Application of multivariate data analysis for food quality investigations: an example-based review, Food Res. Int. 151 (2022) 110878, https://doi.org/10.1016/J.FOODRES.2021.110878.

[47] C.G. Bertinetto, R. Spijkerman, L. Hesselink, G.H. Tinnevelt, C.C.W.G. Bongers, G. J. Postma, M.T.E. Hopman, L. Koenderman, J.J. Jansen, Comprehensive multivariate evaluation of the effects on cell phenotypes in multicolor flow cytometry data using ANOVA simultaneous component analysis, J. Chemometr. 37 (2023) e3402, https://doi.org/10.1002/CEM.3402;WGROUP:STRING:PUBLICATION.

[48] Y. Sefid-Sefidehkhan, A. Jouyban, M. Khoshkam, M. Amiri, E. Rahimpour, Application of ASCA as a multivariate statistical tool for identification of critical parameters for spectroscopic determination of dexamethasone, Iran. J. Chem. Chem. Eng. 42 (2023) 2175–2186, https://doi.org/10.30492/IJCCE.2022.560104.5515.

[49] A. Rust, F. Marini, M. Allsopp, P.J. Williams, M. Manley, Application of ANOVA-simultaneous component analysis to quantify and characterise effects of age, temperature, syrup adulteration and irradiation on near-infrared (NIR) spectral data of honey, Spectrochim. Acta A Mol. Biomol. Spectrosc. 253 (2021) 119546, https://doi.org/10.1016/J.SAA.2021.119546.

[50] A. Menżyk, A. Damin, A. Martyna, E. Alladio, M. Vincenti, G. Martra, G. Zadora, Toward a novel framework for bloodstains dating by Raman spectroscopy: how to avoid sample photodamage and subsampling errors, Talanta 209 (2020) 120565, https://doi.org/10.1016/J.TALANTA.2019.120565.

[51] R.J. Barnes, M.S. Dhanoa, S.J. Lister, Standard normal variate transformation and de-trending of near-infrared diffuse reflectance spectra, Appl. Spectrosc. 43 (1989) 772–777, https://doi.org/10.1366/0003702894202201.

[52] A. Savitzky, M.J.E. Golay, Smoothing and differentiation of data by simplified least squares procedures, Anal. Chem. 36 (1964) 1627–1639, https://doi.org/10.1021/ac60214a047.

[53] P.H.C. Eilers, H.F.M. Boelens, Baseline Correction with Asymmetric Least Squares Smoothing, Leiden, 2005. https://www.researchgate.net/publication/228961729_Baseline_Correction_with_Asymmetric_Least_Squares_Smoothing (accessed May 28, 2025).

[54] S. Wold, K. Esbensen, P. Geladi, Principal component analysis, Chemom. Intel. Lab. Syst. 2 (1987) 37–52, https://doi.org/10.1016/0169-7439(87)80084-9.

[55] C. Malegori, P. Oliveri, Principal Component Analysis, in: Hyperspectral Imaging Analysis and Applications for Food Quality, CRC Press, 2018: pp. 85–107. doi:https://doi.org/10.1201/9781315209203-6.

[56] S. Wold, M. Sjöström, L. Eriksson, PLS-regression: a basic tool of chemometrics, Chemom. Intel. Lab. Syst. 58 (2001) 109–130, https://doi.org/10.1016/S0169-7439(01)00155-1.

[57] S. Wold, A. Ruhe, H. Wold, W.J. Dunn III, The collinearity problem in linear regression. The partial least squares (PLS) approach to generalized inverses, SIAM J. Sci. Stat. Comput. 5 (1984) 735–743, https://doi.org/10.1137/0905052.

[58] T. Pham-Gia, Exact distribution of the generalized Wilks's statistic and applications, J. Multivar. Anal. 99 (2008) 1698–1716, https://doi.org/10.1016/J.JMVA.2008.01.021.

[59] S.S. Wilks, Certain generalizations in the analysis of variance, Biometrika 24 (1932) 471, https://doi.org/10.2307/2331979.

[60] R.A. Armstrong, When to use the Bonferroni correction, Ophthalmic Physiol. Opt. 34 (2014) 502–508, https://doi.org/10.1111/OPO.12131.

[61] K.C. Doty, C.K. Muro, I.K. Lednev, Predicting the time of the crime: bloodstain aging estimation for up to two years, Forensic Chem. 5 (2017) 1–7, https://doi.org/10.1016/J.FORC.2017.05.002.
[62] P. Lemler, W.R. Premasiri, A. DelMonaco, L.D. Ziegler, NIR Raman spectra of whole human blood: effects of laser-induced and in vitro hemoglobin denaturation, Anal. Bioanal. Chem. 406 (2014) 193–200, https://doi.org/10.1007/S00216-013-7427-7.
[63] K.C. Doty, G. McLaughlin, I.K. Lednev, A. Raman, "Spectroscopic clock" for bloodstain age determination: the first week after deposition, Anal. Bioanal. Chem. 408 (2016) 3993–4001, https://doi.org/10.1007/s00216-016-9486-z.
[64] N.M. Htun, Y.C. Chen, B. Lim, T. Schiller, G.J. Maghzal, A.L. Huang, K.D. Elgass, J. Rivera, H.G. Schneider, B.R. Wood, R. Stocker, K. Peter, Near-infrared autofluorescence induced by intraplaque hemorrhage and heme degradation as marker for high-risk atherosclerotic plaques, Nat. Commun. 8 (2017), https://doi.org/10.1038/S41467-017-00138-X.
[65] E. Nagababu, J.M. Rifkind, Heme degradation during autoxidation of oxyhemoglobin, Biochem. Biophys. Res. Commun. 273 (2000) 839–845, https://doi.org/10.1006/bbrc.2000.3025.
[66] U. Neugebauer, A. März, T. Henkel, M. Schmitt, J. Popp, Spectroscopic detection and quantification of heme and heme degradation products, Anal. Bioanal. Chem. 404 (2012) 2819–2829, https://doi.org/10.1007/S00216-012-6288-9/METRICS.
[67] R. Dasgupta, S. Ahlawat, R.S. Verma, A. Uppal, P.K. Gupta, Hemoglobin degradation in human erythrocytes with long-duration near-infrared laser exposure in Raman optical tweezers, J. Biomed. Opt. 15 (2010) 055009, https://doi.org/10.1117/1.3497048.
[68] A. Menżyk, A. Damin, A. Martyna, E. Alladio, M. Vincenti, G. Martra, G. Zadora, Toward a novel framework for bloodstains dating by Raman spectroscopy: how to avoid sample photodamage and subsampling errors, Talanta 1 (2020) 120565, https://doi.org/10.1016/j.talanta.2019.120565.
[69] B.R. Wood, L. Hammer, L. Davis, D. McNaughton, Raman microspectroscopy and imaging provides insights into heme aggregation and denaturation within human erythrocytes, J. Biomed. Opt. 10 (2005) 014005, https://doi.org/10.1117/1.1854678.
[70] P. Oliveri, C. Malegori, R. Simonetti, M. Casale, The impact of signal pre-processing on the final interpretation of analytical outcomes – a tutorial, Anal. Chim. Acta 1058 (2019) 9–17, https://doi.org/10.1016/J.ACA.2018.10.055.

Condition	1st derivative + SNV				SNV				Selected pre-processing
	LV	***RMSECV***	***LV****	***RMSECV****	***LV***	***RMSECV***	***LV****	***RMSECV****	
C_HD_I	6	8.5	3	20.7	6	7.8	3	19.1	1st derivative + SNV
C_HD_O	5	9.0	3	15.9	9	6.0	3	15.0	
C_CW_I	6	13.0	3	33.3	5	24.1	3	39.6	
C_CW_O	5	18.2	3	34.2	6	30.5	3	37.1	
G_HD_I	3	34.1	3	34.1	4	29.6	3	32.2	SNV
G_HD_O	4	35.3	3	44.5	6	13.9	3	21.5	
G_CW_I	4	69.5	3	65.0	4	58.8	3	62.0	
G_CW_O	4	45.4	3	43.4	5	28.5	3	42.5	
M_HD_I	3	57.1	3	57.1	5	56.8	3	61.0	1st derivative + SNV
M_HD_O	3	54.5	3	54.5	5	40.6	3	54.3	
M_CW_I	3	54.3	3	54.3	3	68.9	3	68.9	
M_CW_O	4	64.3	3	72.6	5	76.7	3	75.8	
P_HD_I	6	12.3	3	23.4	7	12.1	3	15.5	1st derivative + SNV
P_HD_O	4	23.1	3	26.6	6	15.6	3	17.7	
P_CW_I	4	46.6	3	53.3	5	45.3	3	54.5	
P_CW_O	4	52.7	3	65.2	6	51.5	3	78.1	

Table S1: *Model results for NIR spectroscopy. LV* and RMSECV* represent, respectively, the number of chosen latent variables and the RMSECV of the model when the number of latent variables is equal to LV*.*

Condition	Raw				AWLS				Selected pre-processing
	LV	***RMSECV***	***LV****	***RMSECV****	***LV***	***RMSECV***	***LV****	***RMSECV****	
C_HD_I	3	66.9	3	66.9	2	76.8	2	76.8	Raw
C_HD_O	3	51.8	3	51.8	2	66.2	2	66.2	
C_CW_I	3	36.0	3	36.0	2	61.0	2	61.0	
C_CW_O	3	38.1	3	38.1	3	41.9	2	52.4	
G_HD_I	3	33.3	3	33.3	2	45.5	2	45.5	Raw
G_HD_O	3	29.7	3	29.7	3	33.3	2	42.5	
G_CW_I	4	29.3	3	37.7	3	44.0	2	56.0	
G_CW_O	3	34.4	3	34.4	3	30.0	2	35.4	
M_HD_I	3	24.0	3	24.0	2	40.7	2	40.7	Raw
M_HD_O	3	30.2	3	30.2	2	41.5	2	41.5	
M_CW_I	3	30.8	3	30.8	3	37.2	2	45.0	
M_CW_O	3	34.8	3	34.8	3	34.6	2	39.7	
P_HD_I	3	31.3	3	31.3	3	38.7	2	39.9	Raw
P_HD_O	3	28.1	3	28.1	3	28.0	2	37.8	
P_CW_I	3	30.2	3	30.2	3	36.8	2	46.6	
P_CW_O	3	46.0	3	46.0	3	43.0	2	58.4	

Table S2: *Model results for Raman spectroscopy. LV* and RMSECV* represent, respectively, the number of chosen latent variables and the RMSECV of the model when the number of latent variables is equal to LV*.*

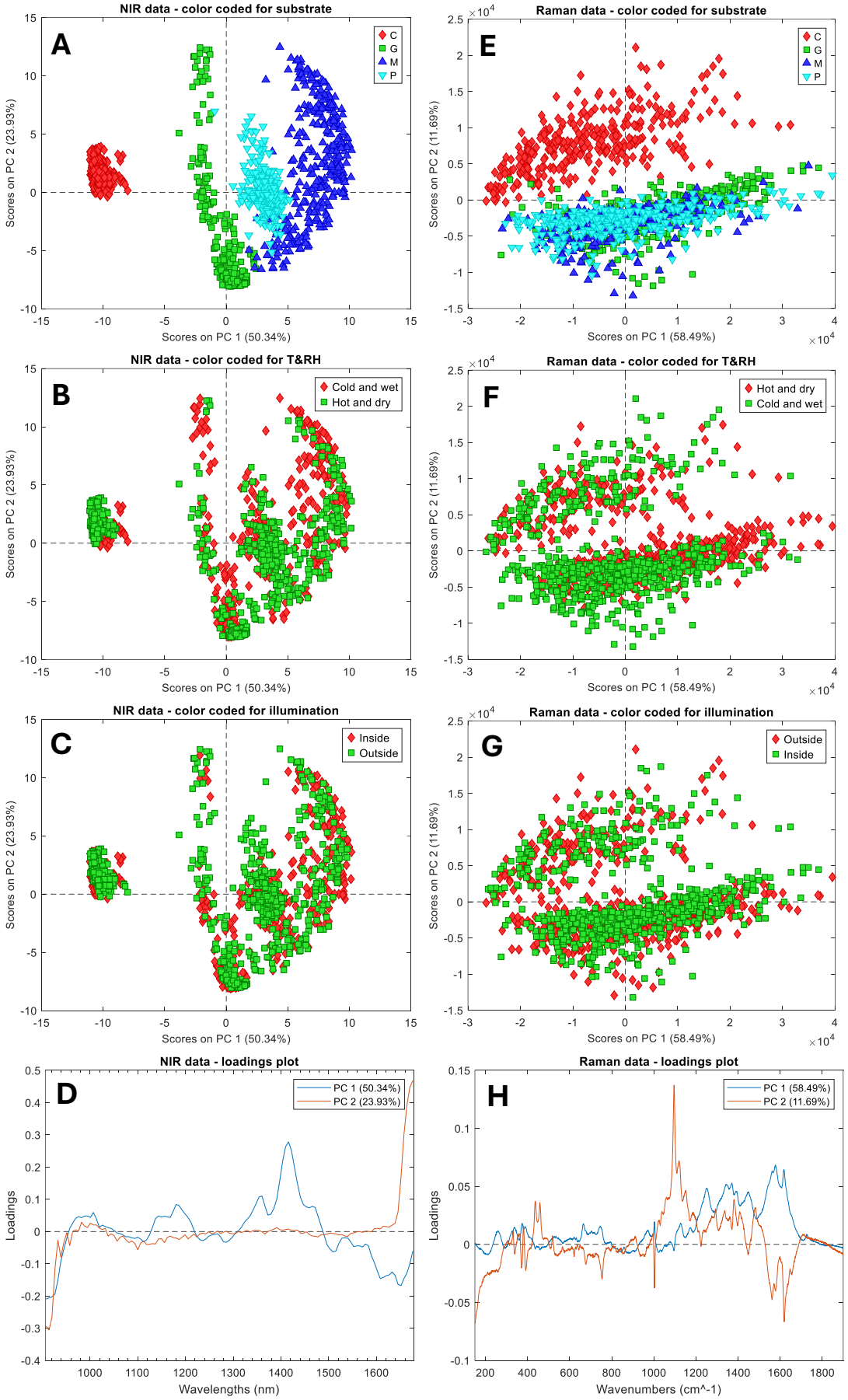

Figure S1: *Scores and loadings plots obtained from PCA on pre-processed data both for NIR and Raman spectroscopies (1st derivative + SNV and AWLS transformed, respectively), colour coded for*

the different factors and levels under analysis. ***A****: NIR score plot colour coded according to substrate (C = cotton, G = glass, M = metal, P = polyblend fabric);* ***B****: NIR score plot colour coded according to T&RH;* ***C****: NIR score plot colour coded according to illumination;* ***D****: NIR loadings plot;* ***E****: Raman score plot colour coded according to substrate (C = cotton, G = glass, M = metal, P = polyblend fabric);* ***F****: Raman score plot colour coded according to T&RH;* ***G****: Raman score plot colour coded according to illumination; H: Raman loadings plot;*

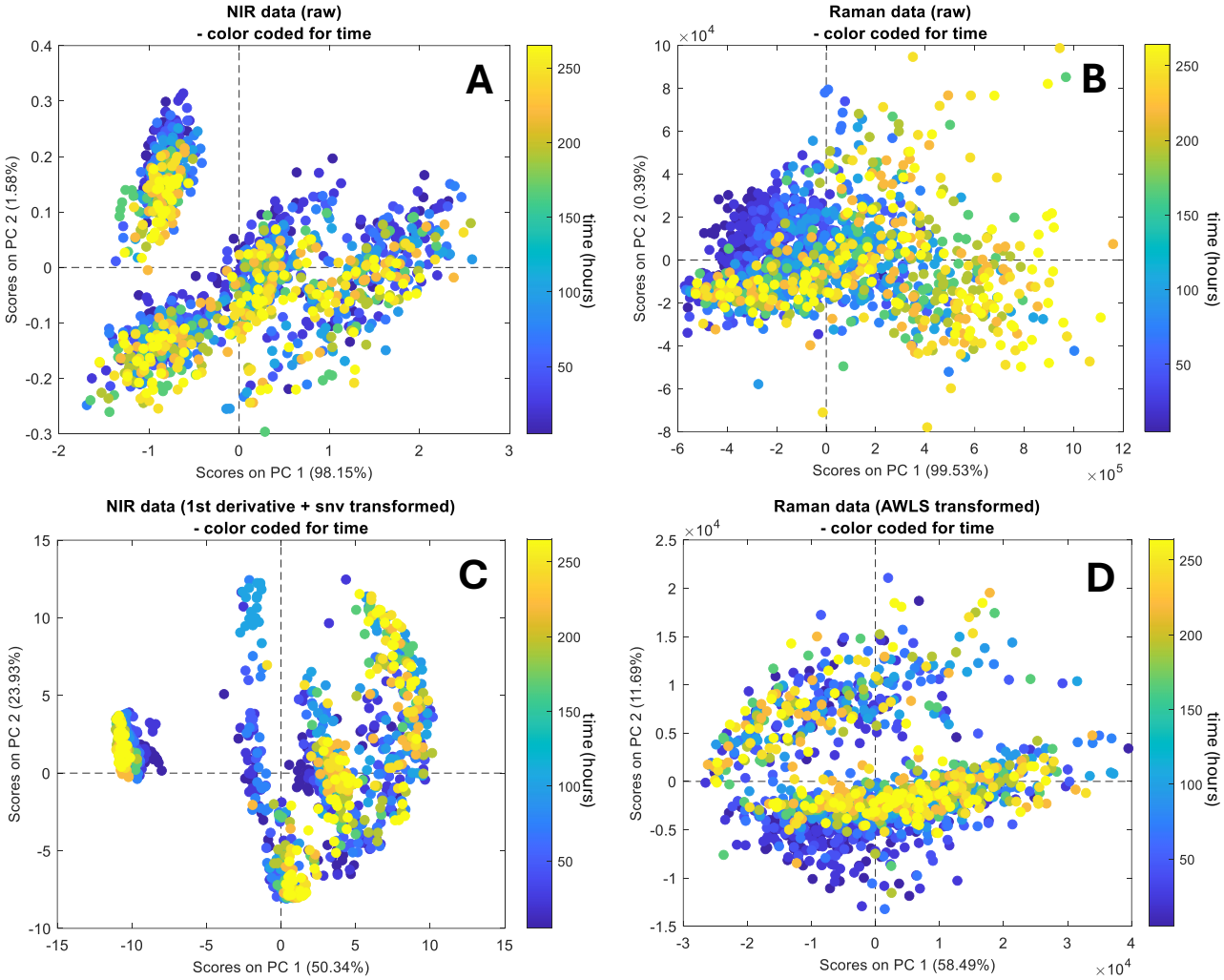

Figure S2: *Score plots colour coded according to measurement time.* ***A****: NIR raw data;* ***B****: Raman raw data;* ***C****: 1st derivative + SNV transformed NIR data;* ***D****: AWLS transformed Raman data.*

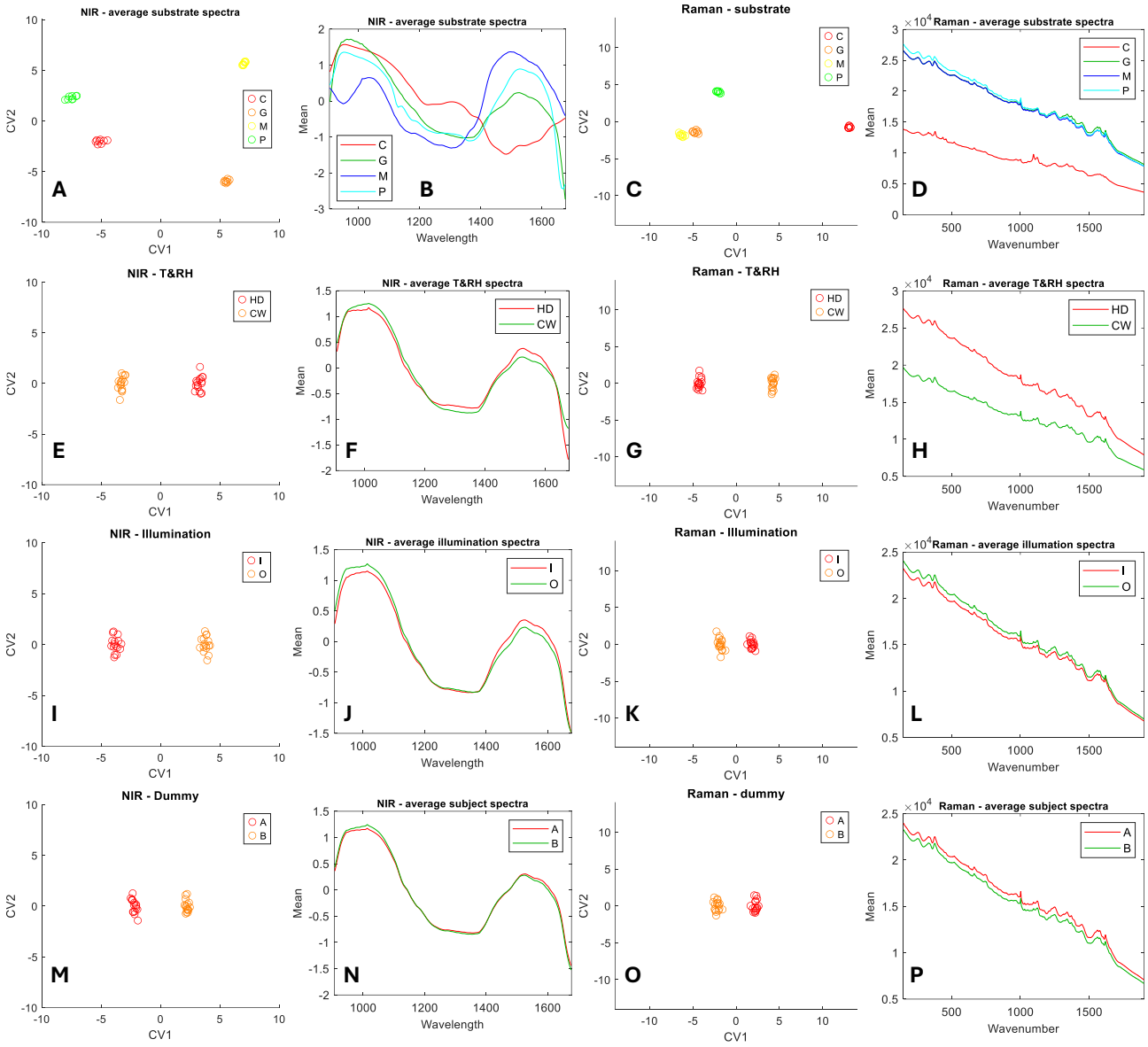

***Figure S3**: RMANOVA scores plot for canonical variates 1 and 2 for all single factors for NIR (**A, E, I, M**) and Raman (**C, G, K, O**) spectroscopies, together with average spectra for each level of each factor for NIR (**B, F, J, N**) and Raman (**D, H, L, P**) spectroscopy.*